Editors' Suggestion

Giant interfacial in-plane magnetic anisotropy in Co/Pt bilayers grown on MgO(110) substrates

Chao Zhou [1,2,*,†] Jia Xu [1,2,*] and Yizheng Wu [2,3,4,‡]

[1]*Department of Physics, School of Physics and Telecommunication Engineering, Shaanxi University of Technology, Hanzhong 723001, China*
[2]*Department of Physics and State Key Laboratory of Surface Physics, Fudan University, Shanghai 200433, China*
[3]*Shanghai Research Center for Quantum Sciences, Shanghai 201315, China*
[4]*Shanghai Key Laboratory of Metasurfaces for Light Manipulation, Fudan University, Shanghai 200433, China*

(Received 10 October 2023; accepted 3 January 2024; published 21 February 2024)

Strong magnetic anisotropy is crucial for spintronic devices, but the strength of in-plane anisotropy (IMA) has constrained its applications in magnetic storage devices in contrast with the perpendicular magnetic anisotropy (PMA). In our study, we observed a giant interfacial uniaxial IMA in Co/Pt(110) bilayers that is approximately five times larger than the PMA in Co/Pt(111) systems. By adding another interface to form Pt/Co/Pt trilayers, the total interfacial uniaxial IMA can be further enhanced to $13.1 \pm 0.3\,\mathrm{erg/cm^2}$, making it a promising platform for high-density storage devices. The interfacial IMA in Co/Pt(110) bilayers is related to the Co at the interface and can be controlled by inserting an ultrathin Cu layer. Our results demonstrated the strong in-plane anisotropy in Co/Pt(110) systems, making it a promising platform for studying the spintronic phenomenon in strongly anisotropic systems.

DOI: 10.1103/PhysRevMaterials.8.024408

I. INTRODUCTION

Magnetic anisotropy, the preference of magnetization to align along specific spatial directions, is a vital aspect of magnetic materials that determines their magnetization configuration and is critical for various applications, such as magnetic recording and spintronic devices [1–3]. Deviation of magnetization from these directions imposes an additional energy penalty on the system, which is the so-called magnetic anisotropy energy (MAE), and provides stability to the magnetization in bulk and film systems. High-density and high-frequency devices require a strong magnetic anisotropy with a large MAE value, which determines the size of basic storage units and the frequency of spintronic devices. Therefore, a large MAE is necessary for those technologies to function properly, making magnetic anisotropy an essential feature.

Extensive studies on both bulk materials and thin films have shown that the most effective recording medium for magnetic storage devices is one with perpendicular magnetic anisotropy (PMA), due to its exceptionally large MAE of up to $\sim 10^7\,\mathrm{erg/cm^3}$. However, for the various magnetoresistance (MR) devices, such as those found in magnetic random-access memory and head assemblies of the hard disk drive, an in-plane magnetized film with uniaxial anisotropy is being used, thus in-plane magnetic anisotropy (IMA) also plays a crucial role in magnetic storage devices [4]. Nevertheless, the MAE of systems with IMA is usually small, with the typical MAE of NiFe being only $\sim 10^3\,\mathrm{erg/cm^3}$ and that of CoFe being $\sim 10^4\,\mathrm{erg/cm^3}$, which is four orders of magnitude smaller than that of the PMA systems. Thus, it would be fundamentally interesting to explore systems with IMA that exhibit large MAE for future MR devices.

The most common approach to induce a strong IMA in magnetic films is interface engineering, which is characterized by the interfacial MAE. This involves growing the films on special surfaces, such as vicinal surfaces [5–7], obliquely sputtered films [8], and nanopatterned structures [9,10]. Another alternative method is to grow the magnetic film on specialized systems, such as GaAs(001) [11,12], heavy metals [13–15], and antiferromagnetic or ferrimagnetic bilayers [16–18]. Moreover, the strain can also be used to induce strong IMA in films [19,20].The MAE values provided by these interface engineering techniques are often larger than those provided by bulk effects, so the interface is important to explore the strong IMA system. However, interfacial MAE can only be achieved up to $\sim 1\,\mathrm{erg/cm^2}$ at room temperature for the system with IMA, which corresponds to 0.03 meV/atom for common ferromagnetic metals such as Fe or Co, and large interfacial MAE can only be achieved at low temperatures, making it difficult to integrate them into devices [18]. Therefore, there is a great need to explore the IMA material systems that exhibit a large interfacial MAE and can operate at room temperature.

Co/Pt bilayer is a popular choice for spintronic devices due to its strong spin-orbit coupling of heavy metals and the hybridization between Co 3*d* and Pt 5*d* orbitals [21,22], and has recently become a fascinating candidate for investigating many novel phenomena in magnetic anisotropy for systems with different crystal orientations of the Pt layer. For example, the Co/Pt(111) system is well studied and has a large PMA with an interfacial MAE value of up to $1.2\,\mathrm{erg/cm^2}$ [21,22]. The systems containing Pt(110) also presented several anisotropic behaviors, such as self-diffusion [23], spin

*These authors contributed equally to this work.
†zhouchao@snut.edu.cn
‡Corresponding author: wuyizheng@fudan.edu.cn

Hall magnetoresistance [24], and terahertz emission [25]. Due to the twofold structural symmetry of the Pt(110) surface, the associated spin-orbit coupling should contain a twofold symmetry. This inherent symmetry has the potential to induce strong in-plane uniaxial anisotropy. Such phenomenon has been experimentally confirmed in various systems, including the in-plane anisotropy in Pt at the Co/Pt(110) interface [26], the potential of anisotropic Dzyaloshinskii-Moriya interaction in Co/Pt(110) [27], and Co/Pt(110) superlattices [28]. Notably, similar observations of IMA have been reported in Co films on other heavy metal (110) surfaces [28]. However, there is still a lack of systematical studies on the Co thickness dependence of IMA and quantitative extraction of MAE in Co/Pt(110) systems.

In this work, we demonstrate a significant IMA with interfacial MAE values as high as ∼5–6 erg/cm^2 in the Co/Pt(110) system at room temperature, which is approximately five times larger than the PMA in Co/Pt(111) systems. We investigated the lattice structure of the Co film in this system and observed a gradual structure transition from the face-centered-cubic (fcc) phase to the hexagonal close-packed (hcp) phase, which is independent of large IMA in this system. Our results also show that by introducing an ultrathin Cu layer at the Co/Pt interface, the easy axis of the IMA can be manipulated, and that the strength of MAE can be further enhanced twice by forming a Pt/Co/Pt sandwich structure. Our findings provide a promising platform for realizing magnetic storage devices with strong in-plane magnetization, which could advance spintronics magnetic storage devices.

II. EXPERIMENTS

The samples used in this study were grown on MgO(110) substrates in an ultrahigh vacuum (UHV) system by molecular beam epitaxy (MBE), with a base pressure of 2×10^{-10} Torr [25]. The single-crystal MgO(110) substrates were ultrasonically cleansed with acetone and alcohol. After being transferred into the UHV chamber, the substrates are annealed at 700 °C for half an hour inside the UHV chamber. The first 1-nm-thick Pt film was deposited at 550 °C, and the remaining Pt layer was grown at room temperature (RT) by pulsed laser deposition (PLD) [25]. The Co or Cu layer was subsequently prepared on top of the Pt layer at RT via the MBE growth. To investigate the thickness dependence of the sample, the film was grown into a wedge or step shape by moving the substrate behind a knife-edge shutter. Finally, a 5-nm MgO protective layer was deposited before the sample was taken out of the UHV chamber. The film thickness was determined by monitoring the deposition rate, which was approximately 0.2 nm/min, using a calibrated quartz thickness monitor.

To investigate the interface crystal structure in the Co/Pt bilayer, we used high-resolution transmission electron microscopy (HR-TEM) to measure the cross-section structure of samples. The HR-TEM measurements were performed by a commercial company [Material Science Laboratory of SAE Technologies Development (Dongguan) Co., Ltd] using an electron microscope operating at an acceleration voltage of 200 kV.

The longitudinal magneto-optical Kerr effect (MOKE) measurements were performed at RT using a laser diode with a wavelength of 670 nm. The rotating-of-field magneto-optical Kerr effect (ROTMOKE) technique was used to determine the magnetic anisotropies at RT with a magnetic field rotating in the sample plane [29]. The measurements were carried out using a small laser beam with a diameter below 0.2 mm, allowing for thickness-dependent studies on the wedge-shaped sample with the Co thickness (d_{Co}) ranging from 0 to 30 nm with a slope of 4 nm/mm. Magnetization hysteresis loops with a field up to 7 T along different orientations were measured using a superconducting quantum interference device (SQUID) from the Quantum Design company. To determine the volume of Co film precisely, the Co/Pt(110) films were fabricated into 1×1 mm^2 squares by photolithography.

III. RESULTS AND DISCUSSION

A. Sample structure characterization

To study the structural properties of Co/Pt(110) bilayers, we utilized *in situ* reflection high-energy electron diffraction (RHEED) imaging during the bilayer growth to observe the surface structures, using incident electron beams along both MgO[001] and [1$\bar{1}$0] directions. The well-ordered MgO(110) surface was confirmed by sharp patterns, as shown in Figs. 1(a) and 1(b). The RHEED images revealed the presence of some small crystalline islands on the MgO film during the growth of the initial 1-nm Pt layer, as shown in Figs. 1(c) and 1(d). As the Pt thickness increased, the RHEED patterns gradually developed into sharp-stripe shape for $d_{\mathrm{Pt}} > 1$ nm and then became stable for $d_{\mathrm{Pt}} > 5$ nm, indicating good epitaxial growth of the Pt film with the fcc structure on MgO(110) substrate, as shown in Figs. 1(e) and 1(f) [25]. The x-ray diffraction (XRD) curve measured from a Pt(10 nm)/MgO(110) film is depicted by the red line in Fig. 2(d). Only the MgO(220) and the Pt(220) Bragg peak can be observed, supporting the epitaxial growth relation of Pt[001](110)$_{\mathrm{fcc}}$ ∥ MgO[001](110)$_{\mathrm{fcc}}$ [25].

The Co thickness-dependent RHEED images from Co(d_{Co})/Pt(10 nm)/MgO(110) film were also studied as shown in Figs. 1(g)–1(j). Previous studies have reported that the Co film grown on MgO(110) has the mixed structure of fcc and hcp phase [30]. To investigate this, we calculated the corresponding diffraction patterns from the fcc-Co(110) and the hcp-Co(1$\bar{1}$00) surface as shown in Figs. 1(m) and 1(n) [31], which agreed well with experimental patterns, indicating the 3-nm Co film should have the fcc structure [32], and the 30-nm Co film should have the hcp structure. The XRD measurement from 30 nm Co is also depicted by the black line shown in Fig. 2(d); both hcp-Co(1$\bar{1}$00) and fcc-Co(220) peaks can be observed, suggesting the existence of both those phases, and the sharp hcp Co(1$\bar{1}$00) peak indicates the dominant hcp structure in the film. The result suggested a structure transition from fcc to hcp while increasing the Co film thickness, which may be attributed to the lattice relaxation of the film [31].

We analyzed the line profiles of RHEED patterns with the electron beam along MgO[1$\bar{1}$0] at the red dashed lines in Fig. 1. The fcc Co showed three major peaks while two new peaks appeared for hcp Co between them. In Fig. 2(a), we displayed a color plot of the d_{Co}-dependent line profiles,

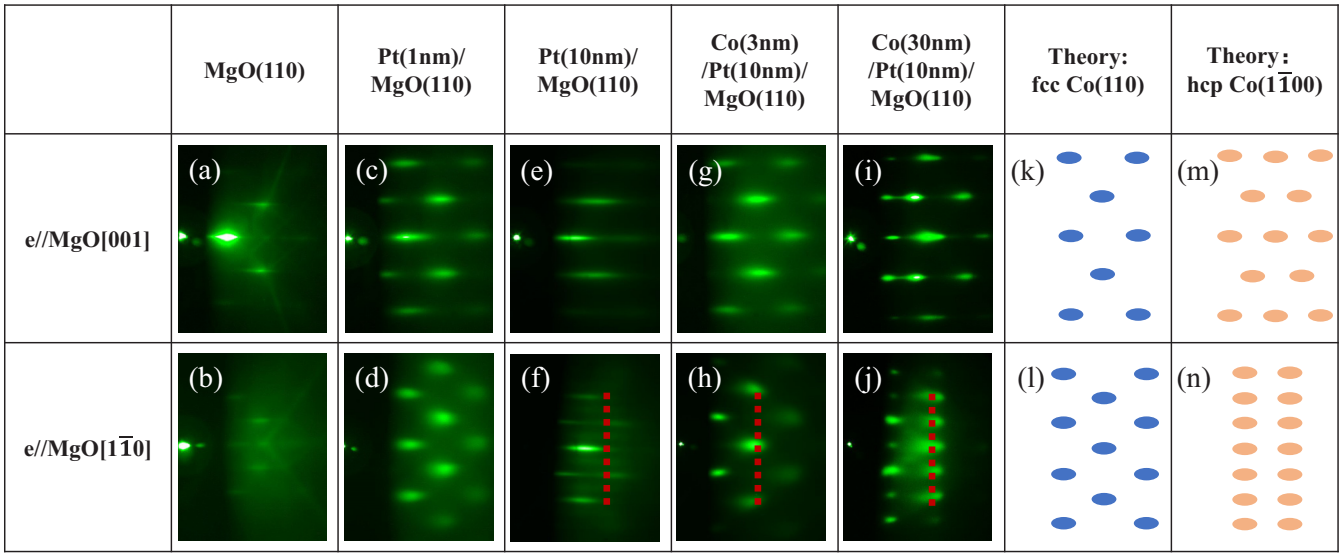

FIG. 1. (a)–(j) RHEED patterns for thin films grown on MgO(110) substrates taken with incident electron beam along two crystallographic directions: MgO[110] direction (upper row) and MgO[1$\bar{1}$0] direction (lower row). Red dashed lines in panels (f), (h), and (j) indicate the position for line profile extraction and analysis. (k)–(n) Calculated RHEED patterns for face-centered cubic (fcc) structure (k)–(l), and hexagonal close-packed (hcp) structure (m) and (n).

and found that line 1 represents the new peaks from hcp Co. Thus, we could choose line 1 to represent the diffraction signal from the hcp Co, and line 2 to represent the mixed diffraction signal from both fcc and hcp structures. Figure 2(b) shows the extracted d_{Co}-dependent intensity I_1 and I_2 from lines 1 and 2 in Fig. 2(a), respectively, and the ratio between I_2 and I_1 as shown in Fig. 2(c). It indicated the ratio increased with d_{Co} and reached a maximum at $d_{Co} \sim 1.5$ nm, corresponding to the fully developed fcc-Co film. The decrease of the ratio for $d_{Co} > 1.5$ nm was due to the gradual evolution of the hcp-Co structure, which fully developed at $d_{Co} \sim 6$ nm. Hence, the fcc Co could only exist near the Co/Pt interface with a maximum thickness of 1.5 nm.

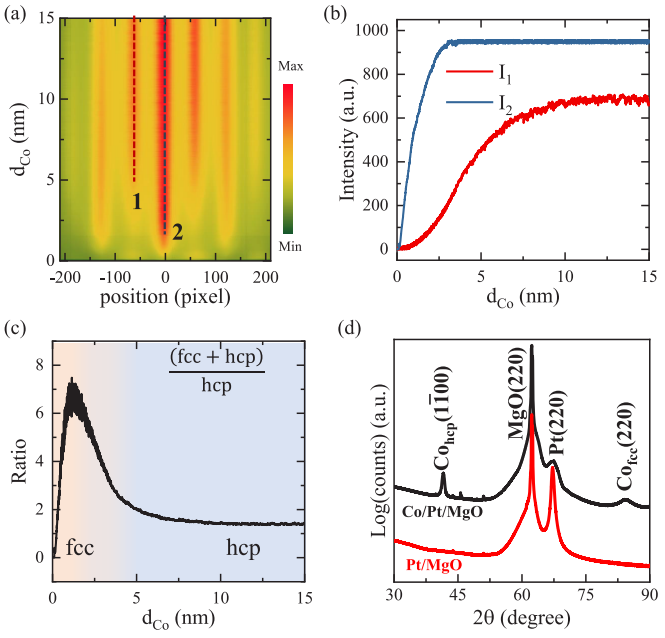

FIG. 2. (a) The d_{Co}-dependent line profiles of RHEED images for Co film grown on a 10-nm Pt(110) film. (b) Corresponding d_{Co}-dependent RHEED intensities along the dashed lines in (a). (c) The ratios of two lines in (b), indicating the transition of Co structure from fcc to hcp. (d) X-ray diffraction spectrum from Co(20 nm)/Pt(10 nm)/MgO(110) and Pt(10 nm)/MgO(110).

To further verify that the fcc Co only exists in the interface, cross-sectional transmission electron microscopy (TEM) measurement was also performed on a MgO(10 nm)/Co(5 nm)/Pt(10 nm)/MgO(110) sample. The high-angle annular dark-field scanning transmission electron microscopy (HAADF-STEM) image in Fig. 3(a) demonstrates a sharp Co/Pt interface. The high-resolution image in Fig. 3(b) at the Co/Pt interface from the area marked by the red dashed box in Fig. 3(a), revealed that both Pt and Co layers had clear fcc lattices near their interface, as shown by the blue circles. We conducted the fast Fourier transform (FFT) analysis and found that the derived FFT patterns in Fig. 3(c) from the MgO substrate, Pt layer, and thin Co layer near the Co/Pt interface ($d_{Co} \sim 0.5$–3 nm) are very similar. However, as indicated by the dashed ovals, the FFT pattern in the Co layer away from the Co/Pt interface ($d_{Co} \sim 3.5$–5 nm) shows the additional spots which could be attributed to the hcp-Co structure. Thus, the TEM result further confirms that only the Co layer near the Co/Pt interface has the fcc structure.

B. Quantification of strong magnetic anisotropy in Co/Pt(110) bilayer

We used longitudinal MOKE measurement to investigate the d_{Co} dependence of in-plane magnetic properties at RT, with a maximum external magnetic field of 2.5 kOe applied in the film plane. Hysteresis loops were obtained from Co(d_{Co})/Pt(10 nm)/MgO(110) film as a function of d_{Co}, with the field H applied along the MgO[001] and [1$\bar{1}$0] direction, respectively, as shown in Figs. 4(a) and 4(b). The

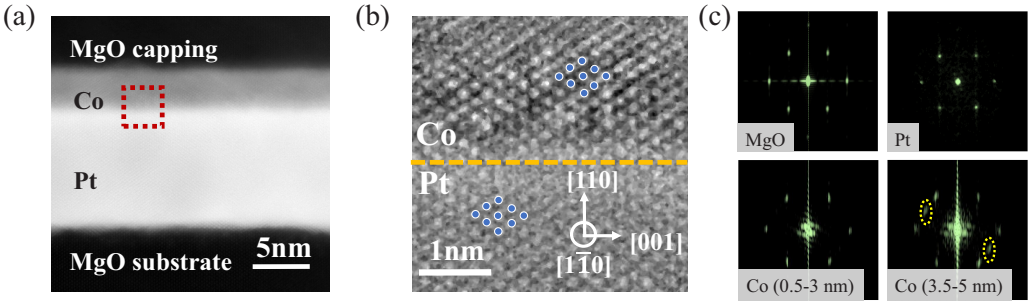

FIG. 3. (a) Dark-field TEM cross-section image of a Co(5 nm)/Pt(10 nm)/MgO(110) sample. (b) High-resolution TEM images displaying atomic structures near the Co/Pt surface, with blue circles marking the Pt and Co atoms, confirming the fcc structure. (c) The FFT patterns from TEM images of the MgO substrate, Pt underlayer, Co layer near the Co/Pt interface, and 3.5-nm Co film away from the Co/Pt interface.

hysteretic loops exhibited a typical rectangular easy-axis (EA) loop for the field applied along $H \parallel$ MgO[001] direction and hard-axis (HA) loops with irregular asymmetric shapes for $H\|$/MgO[1$\bar{1}$0]. The nonsymmetric shapes in the HA loops may arise from both higher-order magnetic anisotropies with odd orders [33] and quadratic Kerr contributions [34]. These results suggest that there is a uniaxial IMA in the Co/Pt(110) system with EA along the MgO[001] direction. The saturation field H_s for the $H\|$ [1$\bar{1}$0] scan is more than four times larger than that for the $H \parallel$ [001] scan at the same Co thickness, indicating the strong uniaxial IMA in the Co/Pt(110) system.

Furthermore, we found that the hysteresis loops strongly depend on the Co thickness, with the magnetization being harder to saturate at thinner Co thickness, indicating the existence of Co thickness-dependent strong uniaxial IMA in the Co/Pt(110) bilayers. However, these results cannot provide quantitative information on the MAE, which is crucial to the development of magnetic storage devices. Thus, we performed Co-thickness-dependent ROTMOKE measurement within a rotatable magnetic field, which has proven an ideal and direct probe to the MAE in magnetic films. For a single-crystalline Co/Pt(110) system, there will be a fourfold anisotropy and a uniaxial magnetic anisotropy according to the results shown in Figs. 4(a) and 4(b).

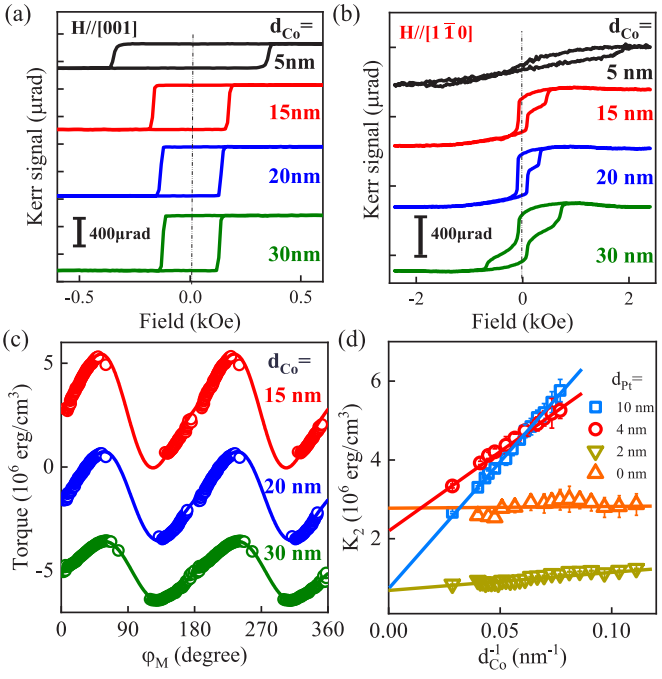

FIG. 4. (a), (b) Representative hysteresis loops obtained by Kerr signal for Co(d_{Co})/Pt(10 nm) with field H applied along (a) MgO[001] and (b) MgO[1$\bar{1}$0] direction at room temperature. (c) Typical torque curves with varying d_{Co}, and solid lines represent fitting curves using Eq. (1). (d) The determined d_{Co}^{-1}-dependent K_2 with different underlayer thickness d_{Pt}. The solid lines show the linear fitting.

Under a strong enough magnetic field, the torque acting on the Co magnetization due to the external field H is equal in magnitude to the magnetic anisotropies. The balancing torque τ equation can be written as

$$\tau = M_S H \sin(\varphi_H - \varphi_M) = K_2 \sin 2(\varphi_M - \varphi_2) + \frac{K_4}{2} \sin 4(\varphi_M - \varphi_4), \quad (1)$$

where the left-hand side is the torque from the magnetic field, and M_S is the saturation magnetization and φ_H (φ_M) is the angle between $\vec{H}$ ($\vec{M}$) and the MgO[001] direction. The right-hand side represents the torques from in-plane uniaxial anisotropy and fourfold anisotropy, with φ_2 (φ_4) representing the angles between the easy axes of uniaxial (fourfold) anisotropy and MgO[001], respectively. The torque τ can be determined experimentally because both H and φ_H are experimental parameters, and φ_M can be determined by the MOKE signal. Therefore, by taking the bulk value of Co magnetization M_S, K_2 and K_4 can be obtained by fitting the τ curve using Eq. (1).

Figure 4(c) shows the torque curves obtained from ROTMOKE measurements for Co/Pt(110) bilayer with different Co thicknesses. These curves are well described by Eq. (1), revealing a twofold anisotropy with an EA oriented along the MgO[001] direction ($\varphi_2 = 0°$) and a weak fourfold symmetry with EA deviating 45° from the MgO[001] direction ($\varphi_4 = 45°$). We use a value of $M_S = 1.58\mu_B$/atom for the saturation magnetization, which is derived from literature data for the bulk Co with a hcp structure [35]. This choice is justified by our RHEED measurements (Fig. 1), which indicate that the Co films studied here ($d_{Co} > 13$ nm) are mostly composed of the hcp phase. From the fitting results, we determined the values of K_2 and K_4, which reflect the MAE of

twofold and fourfold anisotropy, respectively. We found that K_4 remains roughly constant at $\sim(1.4-0.6)\times10^6$ erg/cm^3 for all Co thicknesses, while K_2 strongly depends on d_{Co}, with a value of $\sim2.1\times10^6$ erg/cm^3 for $d_{Co}=30$ nm and $\sim5.1\times10^6$ erg/cm^3 for $d_{Co}=15$ nm.

The magnetic anisotropy in ultrathin films is known to have both interfacial and volume contributions [11]. To distinguish between these contributions in the Co/Pt(110) bilayer, we quantitatively analyzed K_2 as a function of the Co thickness for different Pt thicknesses, as shown in Fig. 4(d). The data demonstrate a clear $1/d_{Co}$ dependence, and K_2 can be well fitted by the equation

$$K_2 = K_2^B + K_2^S/d_{Co}, \tag{2}$$

where K_2^B and K_2^S are the intercept and slope, respectively, which represent the volume and interfacial contribution to the MAE.

Our fitted results reveal that the bulk contribution K_2^B is small, with a value of about $(0.7\sim1.4)\times10^6$ erg/cm^3 for all Pt thicknesses, and the anisotropy in the system is dominated by the interfacial contribution. Specifically, we find that the Pt underlayer significantly enhances the interfacial contribution K_2^S. In fact, a Co film without Pt underlayer shows very little interfacial IMA with $K_2^S=0.03$ erg/cm^2, whereas a strong interfacial IMA with K_2^S of 6.4 erg/cm^2 is obtained for Co/Pt(10 nm) bilayer. It is worth noting that the typical MAE of interfacial PMA in Co/Pt(111) films is less than 1.2 erg/cm^2 [14,22], which means that the interfacial IMA in the Co/Pt(110) system is already more than four times larger than the PMA in the Co/Pt(111) systems. Moreover, the strength of interfacial IMA in the Co/Pt(110) system is found to be dependent on d_{Pt}, which could be attributed to the surface structure of Pt film. Our RHEED measurements indicate the surface morphology of the Pt layer changes greatly with the Pt thickness in the thin region.

C. The strong interfacial magnetic anisotropy for ultrathin Co layer

The ROTMOKE measurements were performed on the films with $d_{Co}>5$ nm, where the Co film should be dominated by hcp structure. Previous reports have shown that the anisotropies of hcp-Co(1$\bar{1}$00) and fcc-Co(110) films are significantly different [36]. As the Co structure in the Co/Pt(110) system gradually develops from fcc-Co(110) to hcp-Co(1100) with increasing the Co thickness, it is desired to investigate whether the strong interfacial IMA can change with the film thickness. The RHEED analysis in Fig. 2 shows that the hcp-Co(1100) structure dominates in the film with $d_{Co}>1.5$ nm, thus we prepared the Co/Pt(10 nm)/MgO(110) samples with the Co layer growing into the step shape with different thicknesses of 1, 2, 5, and 6 nm under the same condition. Due to the strong interfacial anisotropy, the saturation fields of the HA loop in these samples are expected to be very strong. Therefore, we performed the magnetization loop measurements in a SQUID system with a field up to 7 T. All samples with different d_{Co} were fabricated into 1×1 mm^2 squares by photolithography, enabling us to determine the volume of Co film precisely for quantifying the magnetization in each sample.

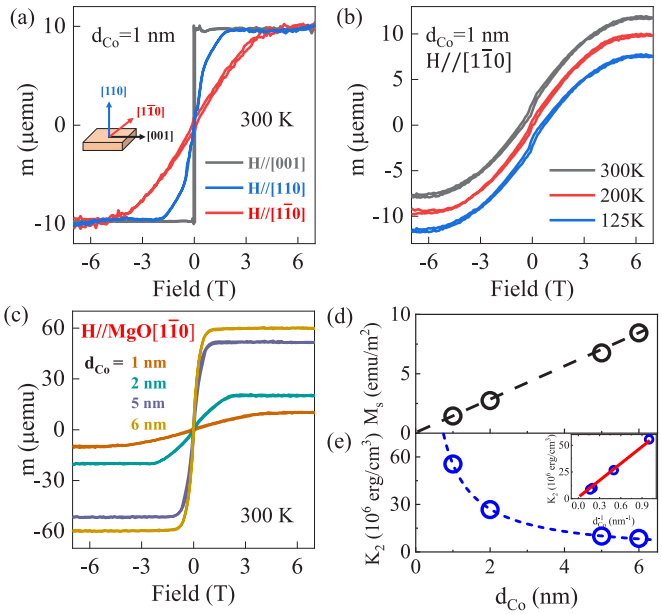

FIG. 5. (a) SQUID measurement of hysteresis loops in the Co(1 nm)/Pt(10 nm) bilayer with H applied along three orthogonal directions at room temperature. (b) Temperature-dependent hysteresis loops in Co(d_{Co})/Pt(10 nm) films with H applied along MgO[1$\bar{1}$0] direction. (c) Thickness-dependent hysteresis loops in Co(d_{Co})/Pt(10 nm) films with the field along MgO[1$\bar{1}$0] direction. (d) Measured d_{Co}-dependent magnetization M_S, with the dashed line indicating the linear fitting. (e) The d_{Co}-dependent uniaxial anisotropy energy, and the dashed line is the d_{Co}^{-1} fitting. The inset in (e) shows the uniaxial anisotropy energy is inversely proportional to d_{Co}.

Figure 5(a) shows the typical hysteresis loops measured at RT from the Co(1 nm)/Pt(10 nm)/MgO(110) sample under the field H applied along the out-of-plane direction (MgO[110]) and two orthogonal in-plane directions (MgO[001] and [1$\bar{1}$0]). We removed the linear diamagnetic background due to the MgO substrate, which was determined by the linear fitting for $H>5.5$ T. The loop with H along MgO[001] shows a typical EA loop, and the loops with $H\parallel$ MgO[1$\bar{1}$0] and $H\parallel$[110] show the typical hard-axis loops. The saturation field is $\sim$4.8 T for $H\parallel$ MgO[1$\bar{1}$0], which is much larger than that of $\sim$1.9 T for $H\parallel$ MgO[110] with the field perpendicular to the film. This result indicates that the in-plane anisotropy is significantly larger than the shape anisotropy in the Co film. The in-plane anisotropy in the Co/Pt(110) has little temperature dependence, as the in-plane HA loops measured at different temperatures are very similar, as shown in Fig. 5(b).

Figure 5(c) shows the in-plane HA loops at RT with varying Co thickness d_{Co}, and Fig. 5(d) shows the determined magnetization moments which increase linearly with d_{Co}. As a result, the Co magnetization can be quantified as $(1.64\pm0.04)\mu_B$/atom, which is close to the bulk value of fcc Co ($1.65\mu_B$/atom) [37] and is only slightly larger than that of hcp Co ($1.58\mu_B$/atom) [35]. However, Fig. 5(c) indicates that the saturation field H_S in the hysteresis loops decreases as d_{Co} increases. According to the Stoner-Wohlfarth model, the MAE of uniaxial anisotropy K_2 can be determined from H_S with the relation $H_S=2K_2/M_S$ [38]. Figure 5(e) shows the determined thickness dependence of K_2, which is inversely

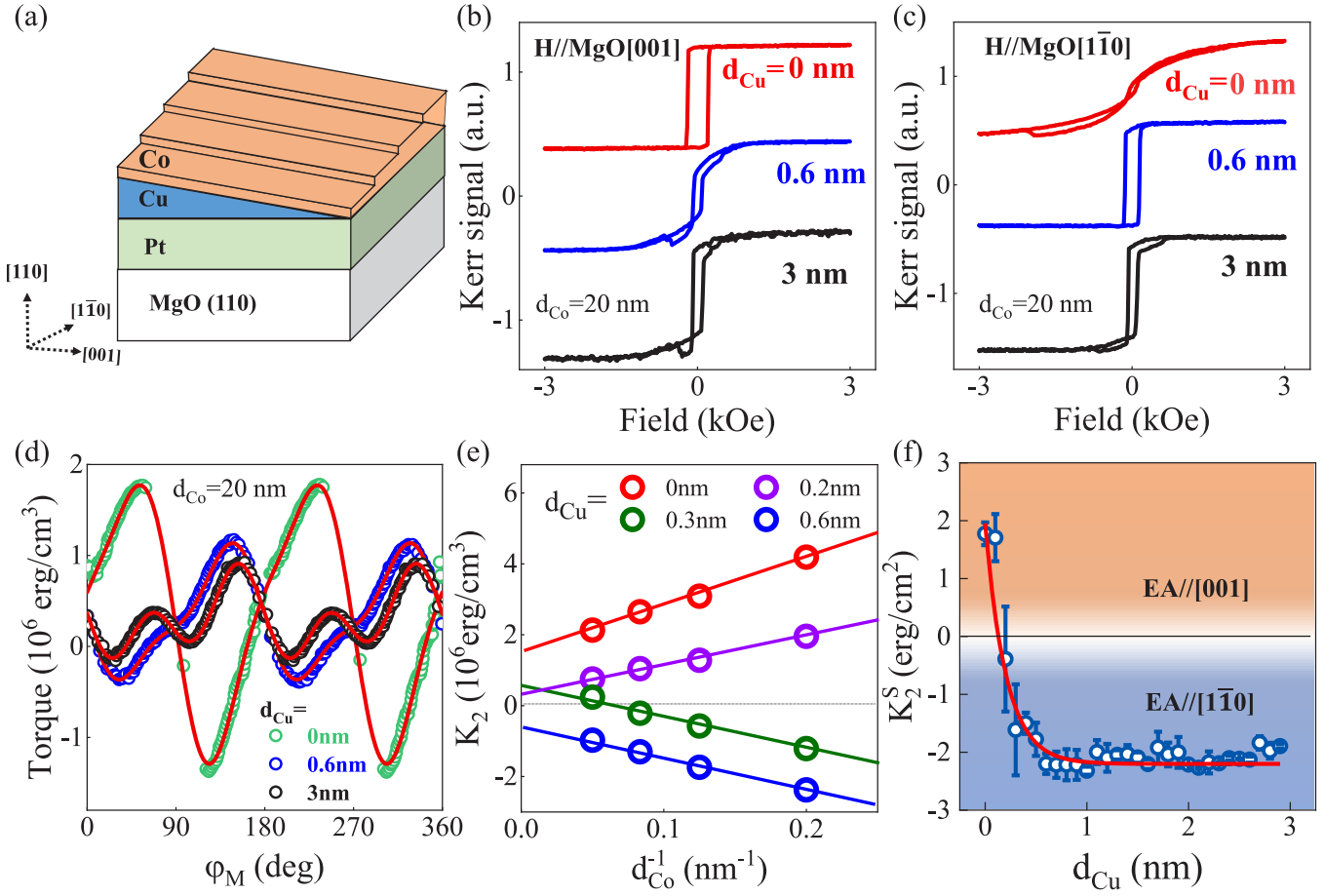

FIG. 6. (a) Schematic diagram of the Co/Cu/Pt(110) sample structure. (b), (c) Typical hysteresis loops of Co(20 nm)/Cu(d_{Cu})/Pt with different d_{Cu} with H applied along MgO[001] and MgO[1$\bar{1}$0] direction, respectively. (d) The typical torque curves of Co(20 nm)/Cu(d_{Cu})/Pt(10 m) trilayers measured by ROTMOKE, with the solid red line representing the fitting using Eq. (1). (e) The d_{Co}^{-1}-dependent uniaxial anisotropy energy K_2 with different Cu interlayer thicknesses. The solid lines are linear fitting. (f) Interfacial uniaxial anisotropy energy K_2^S as a function of d_{Cu}, with the red line representing the exponential fitting.

proportional to d_{Co}, as further proved by the $1/d_{Co}$ linear dependence shown in the inset. Notably, the Co structure gradually changes from fcc into hcp for $d_{Co} > 1.5$ nm, but the data in Fig. 5(e) shows a simple $1/d_{Co}$ dependence, indicating that the strong IMA is independent of structure in Co film away from the interface. The interfacial contribution of MAE K_2^S is determined as $\sim$5.4 erg/cm^2, which is close to the result from ROTMOKE measurement ($\sim$6.4 erg/cm^2) for thick Co layer with hcp structure.

To further confirm that the interfacial anisotropy is independent of the Co structure evolution, we also measured the IMA in Co/Pt(2 nm) bilayers using the torque method determined by analyzing the planar Hall effect (PHE) [18]. In this case, the thickness of Pt was fixed at 2 nm for transport measurements. The Co film was grown into a wedge shape with a thickness range between 0 and 8 nm, and the RHEED results in Fig. 2 suggest a fcc to hcp structure transition. Our measurements demonstrate that the determined K_2 exhibits an excellent $1/d_{Co}$ dependence over the entire thickness range. So, our results highlight the importance of the fcc-Co(110)/Pt(110) interface in forming the strong interfacial IMA, and suggest that the large interfacial IMA in the Co/Pt(110) system is independent of the Co thickness, which is reasonable since the structure at the Co/Pt interface remains unchanged during the Co growth. As both Co and Pt layers have the fcc structure, further theoretical studies are necessary to understand why the fcc Co at the Co/Pt(110) interface has such a large interfacial IMA in the future.

D. Modulation of uniaxial IMA in Co/Pt(110)

To confirm the interfacial origin of the strong IMA in Co/Pt(110) bilayer, we inserted a thin Cu spacer layer between the Co and Pt layers. We then investigated the interfacial uniaxial IMA in Co/Cu/Pt/MgO(110) samples with varying Co thicknesses. During the Cu growth, RHEED images showed that the Cu layer can be well epitaxially grown on the fcc Pt(110) surface. To systematically investigate the Cu thickness dependence of the interfacial IMA, we grew the Cu film into a wedge shape with a thickness range of 0–3 nm and a slope of 0.5 nm/mm, and the Co layer was grown into four steps with thicknesses of 5, 8, 12 and 20 nm. Figure 6(a) shows the schematic structure of the sample, and all the samples with different Co or Cu thicknesses were prepared under the same condition, which is crucial for investigating the thickness-dependent properties.

Figures 6(b) and 6(c) show the measured typical Kerr loops of 20-nm Co layers with different Cu interlayer thicknesses for $H \parallel$ MgO[001] and $H \parallel$ MgO[1$\bar{1}$0], respectively. The Co/Pt bilayer without the Cu interlayer ($d_{Co} = 0$ nm) exhibits the expected EA loop for $H \parallel$ MgO[001] and the HA loop for $H \parallel$ MgO[1$\bar{1}$0]. However, when the interlayer Cu thickness d_{Cu} exceeds 0.4 nm, the loops with $H \parallel$ MgO[1$\bar{1}$0] take on a distinct square shape, while the loops with $H \parallel$ MgO[001] show the typical HA loops. The results suggest that the Cu interlayer leads to a 90° rotation of the EA from the MgO[001] to the MgO[1$\bar{1}$0] direction. The easy axis of Co/Cu/Pt(110) is different from that of Co/Cu(110) in previous studies [39,40], which might be attributed to the large strain in the Cu layer from the underlying Pt layer.

We further performed ROTMOKE measurements on the Co/Cu/Pt(110) samples as a function of the Cu thickness d_{Cu} on the different Co steps with varying d_{Co}. Figure 6(d) shows the typical torque curves from 20-nm-thick Co layers with different d_{Cu}, revealing an opposite phase after inserting the Cu layer, which corresponds to a 90° switching of EA in the uniaxial IMA. The manipulation of the magnetic easy axis through an ultrathin Cu layer enables the realization of multilevel storage and could facilitate the realization of spin wave diodes [41], which require complex in-plane magnetic domain patterns.

Figure 6(e) shows that all the fitted K_2 values from the samples with the same Cu interlayer thickness have a good $1/d_{Co}$ linear dependence. By linear fitting, we obtain the d_{Cu}-dependent interfacial uniaxial anisotropy K_2^S, as shown in Fig. 6(f). K_2^S quickly drops with the Cu thickness and changes sign at $d_{Cu} \sim 0.3$ nm due to 90° switching of EA, then saturates at $d_{Cu} \sim 0.6$ nm. The measured data in Fig. 5(f) can be well fitted by an exponential decay function $K_2^S(d_{Cu}) = K_{2,\infty}^S + (K_{2,0}^S - K_{2,\infty}^S)\exp(-d_{Cu}/\lambda)$, where $K_{2,0}^S$ and $K_{2,\infty}^S$ represent the interface IMA without the Cu interlayer and with a very thick Cu interlayer, respectively. Here, the K_2^S at $d_{Cu} = 0$ nm is smaller than that shown in Fig. 4, which can be attributed to the different surface quality or the small amount of Cu coverage effect during Cu-wedge growth. The fitted decay constant λ for K_2^S is 0.20 ± 0.07 nm, which is only ~1.6 monolayer of Cu(110) film. Our results suggest that even the coverage of a single layer of Cu atoms on the Pt(110) surface is sufficient to change the interfacial IMA.

It is worth noting that for the Co/Cu/Pt films with $d_{Cu} > 0.6$ nm, a large interfacial IMA with MAE ~2 erg/cm^2 is observed, which is approximately ten times larger than the uniaxial anisotropy for the Co films epitaxied on Cu(110) substrates [5]. Such large interfacial anisotropy should not be related to the Pt layer, as Co and Pt layers are well separated by the Cu layer. However, the Pt layer grown on MgO(110) has a very large in-plane strain, which could also be transferred into the Cu and Co layer [25]. Thus, our study indicates that the strained Co/Cu(110) interface can induce strong interfacial uniaxial anisotropy.

The Co/Pt/MgO(110) system exhibits strong IMA at the Co/Pt interface, and it was expected that this interfacial IMA could be further enhanced in a Pt/Co/Pt(110) trilayer with an additional Co/Pt interface. To investigate this, we prepared a sample on MgO(110) substrate with one half covered with Co/Pt (10 nm) and the other half with Pt (4 nm)/Co/Pt (10 nm),

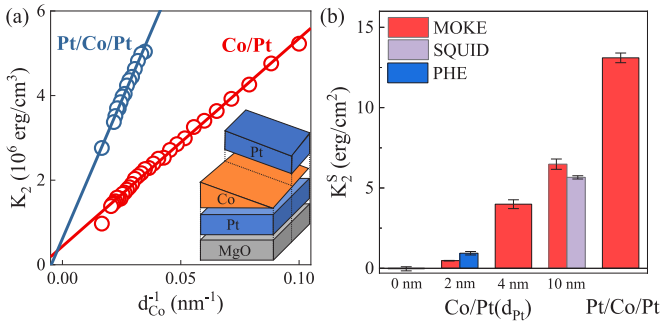

FIG. 7. (a) The uniaxial anisotropy energy K_2 measured by ROTMOKE measurements from Co(d_{Co})/Pt(10 nm) bilayers and Pt(4 nm)/Co(d_{Co})/Pt(10 nm) trilayers, plotted as a function of d_{Co}^{-1}. The solid lines are the linear fitting. (b) Summary of the interfacial uniaxial anisotropy energies obtained from Co/Pt bilayer and Pt/Co/Pt trilayer using various methods.

where the Co layer is grown into a wedge shape, as shown in the inset of Fig. 7(a). Thus, both Pt/Co/Pt trilayer and Pt/Co bilayer were grown under identical conditions, and their MAE of in-plane uniaxial anisotropies were determined through the ROTMOKE measurements. Figure 7(a) shows the measured K_2 as a function of d_{Co}^{-1}, which has a good linear dependence for both samples. The interfacial anisotropy energy K_2^S is quantified as 4.9 ± 0.1 erg/cm^2 for the Co/Pt bilayer and 13.1 ± 0.3 erg/cm^2 for the Pt/Co/Pt trilayer. Since the top of the Co layer has hcp structure when it is thick, the interface of the hcp-Co/Pt(110) interface might also exhibit strong interfacial IMA. In addition, the result suggests that the $[Co/Pt]_n$ multilayer epitaxied on MgO(110) substrate should have both a larger magnetic moment and a stronger interfacial IMA, which is expected to have important implications for the development of magnetic storage devices.

In Fig. 7(b), we summarize all the interfacial MAE K_2^S determined in this work from Co/Pt bilayers and Pt/Co/Pt trilayer. The interfacial PMA in Co/Pt(111) or CoFeB/MgO systems has been widely studied and applied in spintronics devices, but the interfacial MAE typically has a value of 1.1–1.3 erg/cm^2 [21,22,42]. Thus, the MAE of interfacial uniaxial anisotropy in Pt/Co/Pt(110) trilayer is an order of magnitude stronger than that, and also approximately five times stronger than the PMA in Pt/Co/Pt(111) systems. It is worth noting that the MAE of uniaxial IMA in Pt/Co(1 ML)/Pt is estimated to be as high as 2.1×10^9erg/cm^3 (3.61 meV/atom) from our fitted value of K_2^S, which is larger than most of the reported values in continuous films of *3d* metals in both IMA and PMA systems [9,18,43,44]. With such strong IMA, even a nanoisland with a lateral size of (7×7) nm^2 could have an MAE of 1.4 eV, giving the thermal stability factor of $\Delta = K_u V/k_B T \approx 54$ at RT, which satisfies the criteria for 10-year data retention at RT ($\Delta > 45$) [43]. Moreover, it is possible that single atoms or atom clusters of Co on the Pt(110) surface may show even stronger IMA than that in the film system, similar to the PMA in the Co/Pt(111) system [3]. This presents an exciting opportunity to further enhance the IMA and could be valuable for developing future magnetic recording devices with ultrahigh density.

IV. SUMMARY

In summary, our study reported a giant uniaxial IMA with interfacial MAE value of ∼5–6 $\mathrm{erg/cm^2}$ in single-crystalline Co/Pt bilayers grown on MgO(110) substrate, which is about five times larger than PMA in Co/Pt(111) systems. We utilize *in situ* RHEED, XRD, and TEM measurements to characterize the lattice structure and found a phase transition from fcc to hcp structure with increasing Co thickness. The MAE in Co/Pt(110) bilayers exhibits a significant thickness dependence of Co film, indicating a large interfacial IMA related to the fcc Co at the interface, as determined by the ROTMOKE, PHE, and SQUID techniques. The MAE can be further enhanced twice in Pt/Co/Pt sandwich heterostructure. We also found that the easy axis of the uniaxial anisotropy can be rotated by 90° after inserting an ultrathin Cu layer between Co and Pt layers. Our work provides a system for realizing strong in-plane uniaxial anisotropy in thin films, which may serve as a platform for studying the anisotropy in different spin-current effects, such as Dzylashinskii-Moriya interaction, magnetic damping, and electric transport behaviors, and help with the development of new spintronic devices, such as the type-Y spin-orbit torque magnetic random-access memory [45].

ACKNOWLEDGMENTS

This work was supported by the National Key Research and Development Program of China (2022YFA1403300), the National Natural Science Foundation of China (Grants No. 11974079, No. 12274083, No. 12221004, No. 12204296, and No. 12204295), the Shanghai Municipal Science and Technology Major Project (Grant No. 2019SHZDZX01), and the Shanghai Municipal Science and Technology Basic Research Project (Grants No. 22JC1400200 and No. 23dz2260100). Natural Science Foundation of Shaanxi Provincial Department of Education (Grants No. 22JK0321 and No. 22JK0310), Natural Science Basic Research Program of Shaanxi (Grants No. 2022JQ-017 and No. 2023-JC-QN-0077), Shaanxi University of Technology (SLGRCQD2125 and SLGRCQD2215), Youth Hanjiang Scholar Research Support Fund from Shaanxi University of Technology, Open Research Project of State Key Laboratory of Surface Physics from Fudan University (Grant No. KF2022_17), Undergraduate Education and Teaching Reform Research Project at Shaanxi University of Technology (XJG2358), and Curriculum Ideological and Political Education Teaching Reform and Research Project at Shaanxi University of Technology (KCSZ2338).

[1] C. Chappert, A. Fert, and F. N. Van Dau, The emergence of spin electronics in data storage, Nat. Mater. **6**, 813 (2007).

[2] M. Jamet, W. Wernsdorfer, C. Thirion, D. Mailly, V. Dupuis, P. Melinon, and A. Perez, Magnetic anisotropy of a single cobalt nanocluster, Phys. Rev. Lett. **86**, 4676 (2001).

[3] P. Gambardella, S. Rusponi, M. Veronese, S. S. Dhesi, C. Grazioli, A. Dallmeyer, I. Cabria, R. Zeller, P. H. Dederichs, K. Kern, C. Carbone, and H. Brune, Giant magnetic anisotropy of single cobalt atoms and nanoparticles, Science **300**, 1130 (2003).

[4] Q. Shao, P. Li, L. Liu, H. Yang, S. Fukami, A. Razavi, H. Wu, K. Wang, F. Freimuth, Y. Mokrousov, M. D. Stiles, S. Emori, A. Hoffmann, J. Akerman, K. Roy, J.-P. Wang, S.-H. Yang, K. Garello, and W. Zhang, Roadmap of spin–orbit torques, IEEE Trans. Magn. **57**, 1 (2021).

[5] R. K. Kawakami, M. O. Bowen, H. J. Choi, E. J. Escorcia-Aparicio, and Z. Q. Qiu, Effect of atomic steps on the magnetic anisotropy in vicinal Co/Cu(001), Phys. Rev. B **58**, R5924 (1998).

[6] T. Leeb, M. Brockmann, F. Bensch, S. Miethaner, and G. Bayreuther, In-plane magnetic anisotropies in Fe films on vicinal Ag(001) and Au(001) surfaces, J. Appl. Phys. **85**, 4964 (1999).

[7] J. Li, M. Przybylski, F. Yildiz, X. D. Ma, and Y. Z. Wu, Oscillatory magnetic anisotropy originating from quantum well states in Fe films, Phys. Rev. Lett. **102**, 207206 (2009).

[8] R. D. McMichael, C. G. Lee, J. E. Bonevich, P. J. Chen, W. Miller, and W. F. Egelhoff, Strong anisotropy in thin magnetic films deposited on obliquely sputtered Ta underlayers, J. Appl. Phys. **88**, 5296 (2000).

[9] S. A. Mollick, R. Singh, M. Kumar, S. Bhattacharyya, and T. Som, Strong uniaxial magnetic anisotropy in Co films on highly ordered grating-like nanopatterned Ge surfaces, Nanotechnology **29**, 125302 (2018).

[10] S. Ki and J. Dho, Strong uniaxial magnetic anisotropy in triangular wave-like ferromagnetic NiFe thin films, Appl. Phys. Lett. **106**, 212404 (2015).

[11] G. Chen, J. X. Li, J. Zhu, J. H. Liang, and Y. Z. Wu, In-plane magnetic anisotropy in Fe/MgO/GaAs(001) system, J. Appl. Phys. **109**, 07C108 (2011).

[12] G. Bayreuther, J. Premper, M. Sperl, and D. Sander, Uniaxial magnetic anisotropy in Fe/GaAs(001): Role of magnetoelastic interactions, Phys. Rev. B **86**, 054418 (2012).

[13] B. N. Engel, C. D. England, R. A. Van Leeuwen, M. H. Wiedmann, and C. M. Falco, Interface magnetic anisotropy in epitaxial superlattices, Phys. Rev. Lett. **67**, 1910 (1991).

[14] N. W. E. McGee, M. T. Johnson, J. J. de Vries, and J. aan de Stegge, Localized Kerr study of the magnetic properties of an ultrathin epitaxial Co wedge grown on Pt(111), J. Appl. Phys. **73**, 3418 (1993).

[15] H. J. Elmers and U. Gradmann, Magnetic anisotropies in Fe(110) films on W(110), Appl. Phys. A: Solids Surf. **51**, 255 (1990).

[16] J. Zhu, Q. Li, J. X. Li, Z. Ding, C. Y. Won, and Y. Z. Wu, Volume contribution of exchange-coupling-induced uniaxial anisotropy in Fe/CoO/MgO(001) system, J. Appl. Phys. **114**, 173912 (2013).

[17] J. Nogués, D. Lederman, T. J. Moran, and I. K. Schuller, Positive exchange bias in FeF_2-Fe bilayers, Phys. Rev. Lett. **76**, 4624 (1996).

[18] W. N. Cao, J. Li, G. Chen, J. Zhu, C. R. Hu, and Y. Z. Wu, Temperature-dependent magnetic anisotropies in epitaxial Fe/CoO/MgO(001) system studied by the planar Hall effect, Appl. Phys. Lett. **98**, 262506 (2011).

[19] S. Scheibler, O. Yildirim, I. K. Herrmann, and H. J. Hug, Inducing in-plane uniaxial magnetic anisotropies in amorphous CoFeB thin films, J. Magn. Magn. Mater. **585**, 171015 (2023).

[20] S. Isogami and T. Taniyama, Strain mediated in-plane uniaxial magnetic anisotropy in amorphous CoFeB films based on structural phase transitions of $BaTiO_3$ single-crystal substrates, Phys. Status Solidi A **215**, 1700762 (2018).

[21] N. Nakajima, T. Koide, T. Shidara, H. Miyauchi, H. Fukutani, A. Fujimori, K. Iio, T. Katayama, M. Nývlt, and Y. Suzuki, Perpendicular magnetic anisotropy caused by interfacial hybridization via enhanced orbital moment in Co/Pt multilayers: Magnetic circular x-ray dichroism study, Phys. Rev. Lett. **81**, 5229 (1998).

[22] H. Nemoto and Y. Hosoe, Analysis of interfacial magnetic anisotropy in Co/Pt and Co/Pd multilayer films, J. Appl. Phys. **97**, 10J109 (2005).

[23] E. Preuss, N. Freyer, and H. P. Bonzel, Surface self-diffusion on Pt(110): Directional dependence and influence of surface-energy anisotropy, Appl. Phys. A: Solids Surf. **41**, 137 (1986).

[24] R. Thompson, J. Ryu, Y. Du, S. Karube, M. Kohda, and J. Nitta, Current direction dependent spin Hall magnetoresistance in epitaxial Pt/Co bilayers on MgO(110), Phys. Rev. B **101**, 214415 (2020).

[25] C. Q. Liu, W. T. Lu, Z. X. Wei, Y. F. Miao, P. Wang, H. Xia, Y. P. Liu, F. L. Zeng, J. R. Zhang, C. Zhou, H. B. Zhao, Y. Z. Wu, Z. Yuan, and J. Qi, Strain-induced anisotropic terahertz emission from a Fe(211)/Pt(110) bilayer, Phys. Rev. Appl. **15**, 044022 (2021).

[26] J. Alvarez, E. Lundgren, X. Torrelles, H. Isern, K. F. Peters, P. Steadman, and S. Ferrer, Magnetization of Pt in the Co/Pt(110) system investigated with surface x-ray magnetic diffraction: Evidence for in-plane magnetic anisotropy, Phys. Rev. B **60**, 10193 (1999).

[27] Y. Liu, M. D. Kitcher, M. De Graef, and V. Sokalski, Towards hexagonal C_{2v} systems with anisotropic Dzyaloshinkii-Moriya interaction: Characterization of epitaxial Co(10$\bar{1}$0)/Pt(110) multilayer films, Phys. Rev. Mater. **5**, L101401 (2021).

[28] B. Hillebrands and J. R. Dutcher, Origin of very large in-plane anisotropies in (110)-oriented Co/Pd and Co/Pt coherent superlattices, Phys. Rev. B **47**, 6126 (1993).

[29] R. Mattheis and G. Quednau, Determination of the anisotropy field strength in ultra-thin magnetic films using longitudinal MOKE and a rotating field: The ROTMOKE method, J. Magn. Magn. Mater. **205**, 143 (1999).

[30] Y. Nukaga, M. Ohtake, O. Yabuhara, F. Kirino, and M. Futamoto, Epitaxial growth of Co thin films on MgO single-crystal substrates, J. Magn. Soc. Jpn. **34**, 508 (2010).

[31] X. H. Wei, Y. R. Li, J. Zhu, Y. Zhang, Z. Liang, and W. Huang, *In situ* analysis of lattice relaxation by reflection high-energy electron diffraction, J. Phys. D: Appl. Phys. **38**, 4222 (2005).

[32] E. Lundgren, J. Alvarez, X. Torrelles, K. F. Peters, H. Isern, and S. Ferrer, Co/Pt(110) interface: An x-ray-diffraction study, Phys. Rev. B **59**, 2431 (1999).

[33] A. Pokhrel, B. Nepal, U. Karki, A. Sapkota, A. Rai, S. Bey, T. Mewes, and C. Mewes, Influence of layer dependent perpendicular anisotropy on higher-order anisotropies in thin films, J. Magn. Magn. Mater. **563**, 169963 (2022).

[34] J. H. Liang, X. Xiao, J. X. Li, B. C. Zhu, J. Zhu, H. Bao, L. Zhou, and Y. Z. Wu, Quantitative study of the quadratic magneto-optical Kerr effects in Fe films, Opt. Express **23**, 11357 (2015).

[35] H. P. Myers and W. Sucksmith, The spontaneous magnetization of cobalt, Proc. R. Soc. A **207**, 427 (1951).

[36] C. K. Lo, Y. Liou, C. P. Chang, I. Klik, Y. D. Yao, and J. C. A. Huang, Structure and magnetic anisotropy of epitaxial fcc-Co(110) and hcp-Co(1$\bar{1}$00) films, Appl. Phys. Lett. **68**, 2155 (1996).

[37] P. Modak, A. K. Verma, R. S. Rao, B. K. Godwal, and R. Jeanloz, *Ab initio* total-energy and phonon calculations of Co at high pressures, Phys. Rev. B **74**, 012103 (2006).

[38] T. Suzuki, Y. Sugita, M. R. S. Meeting, M. R. S. S. Meeting, B. Clemens, K. Ouchi, and D. Laughlin, *Magnetic Materials: Volume 232: Microstructure and Properties* (Cambridge University Press, Cambridge, UK, 1991).

[39] J. Fassbender, G. Güntherodt, C. Mathieu, B. Hillebrands, R. Jungblut, J. Kohlhepp, M. T. Johnson, D. J. Roberts, and G. A. Gehring, Correlation between structure and magnetic anisotropies of Co on Cu(110), Phys. Rev. B **57**, 5870 (1998).

[40] S. Hope, M. Tselepi, E. Gu, T. M. Parker, and J. A. C. Bland, Two-dimensional percolation phase transition in ultrathin Co/Cu(110), J. Appl. Phys. **85**, 6094 (1999).

[41] J. Lan, W. Yu, R. Wu, and J. Xiao, Spin-wave diode, Phys. Rev. X **5**, 041049 (2015).

[42] S. Ikeda, K. Miura, H. Yamamoto, K. Mizunuma, H. D. Gan, M. Endo, S. Kanai, J. Hayakawa, F. Matsukura, and H. Ohno, A perpendicular-anisotropy CoFeB–MgO magnetic tunnel junction, Nat. Mater. **9**, 721 (2010).

[43] B. Dieny and M. Chshiev, Perpendicular magnetic anisotropy at transition metal/oxide interfaces and applications, Rev. Mod. Phys. **89**, 025008 (2017).

[44] M. T. Johnson, P. J. H. Bloemen, F. J. A. d. Broeder, and J. J. d. Vries, Magnetic anisotropy in metallic multilayers, Rep. Prog. Phys. **59**, 1409 (1996).

[45] S. Fukami, T. Anekawa, C. Zhang, and H. Ohno, A spin–orbit torque switching scheme with collinear magnetic easy axis and current configuration, Nat. Nanotechnol. **11**, 621 (2016).